ELSEVIER

Journal of Power Sources 103 (2002) 293–299

JOURNAL OF POWER SOURCES

www.elsevier.com/locate/jpowsour

$MmNi_{3.55}Co_{0.75}Mn_{0.4}Al_{0.3}B_{0.3}$ hydrogen storage alloys for high-power nickel/metal hydride batteries

Hui Ye*, Yuexiang Huang, Jianxia Chen, Hong Zhang

Division of Energy Science and Technology, Shanghai Institute of Metallurgy, CAS, Shanghai 200050, PR China

Received 4 April 2001; received in revised form 18 June 2001; accepted 16 July 2001

Abstract

Non-stoichiometric La-rich $MmNi_{3.55}Co_{0.75}Mn_{0.4}Al_{0.3}B_{0.3}$ hydrogen storage alloys using B–Ni or B–Fe alloy as additive and Ce-rich $MmNi_{3.55}Co_{0.75}Mn_{0.4}Al_{0.3}B_{0.3}$ one using pure B as additive have been prepared and their microstructure, thermodynamic, and electrochemical characteristics have been examined. It is found that all investigated alloys show good activation performance and high-rate dischargeability though there is a certain decrease in electrochemical capacities compared with the commercial $MmNi_{3.55}Co_{0.75}Mn_{0.4}Al_{0.3}$ alloy. $MmNi_{3.55}Co_{0.75}Mn_{0.4}Al_{0.3}B_{0.3}$ alloys using B–Ni alloy as additive or adopting Ce-rich mischmetal show excellent rate capability and can discharge capacity over 190 mAh/g even under 3000 mA/g current density, which display their promising use in the high-power type Ni/MH battery. The electrochemical performances of these $MmNi_{3.55}Co_{0.75}Mn_{0.4}Al_{0.3}B_{0.3}$ alloys are well correlated with their microstructure, thermodynamic, and kinetic characteristics.

Keywords: Hydrogen storage alloy; Boron addition; Metal hydride electrode; High-rate dischargeability; Electrochemical kinetics

1. Introduction

In a relatively short period of time, hybrid electric vehicles (HEV), in which motive power stems partly from a relatively small internal combustion engine and partly from an electric motor, have emerged and immediately appeared destined to be successful due to its cost-acceptability and high fuel economy [1,2]. The energy density requirements for HEV are relative low. However, specific power and power density requirements for HEV are very high. Nickel/metal hydride (Ni/MH) battery is a strong competition of the power source for HEV market because the system has high specific energy, high-power capability, inherent safety, and design flexibility [3,4]. The power source requirements of power tools and some modern military devices also provide huge market for high-power Ni/MH battery with the phase out of nickel/cadmium battery, which is under the fire of environmental protectionism. To meet with the new power demands of HEV and other high-power applications, much of improvement for Ni/MH batteries, especially concerning with high specific power performance, have to be done. The critical technique is to develop hydrogen storage alloys with superior rate capability.

For the commercial use of $LaNi_5$-type hydrogen storage alloys, multi-component alloying is one of the most effective techniques to tailor properties so as to meet the requirement of Ni/MH batteries [5–7]. Some studies showed that by deviating $LaNi_5$-type compound composition from stoichiometry ratio [8–10] and the addition of boron [11] are very efficient to enhance the rate capability of $LaNi_5$-type hydrogen storage alloys. In the recent, we have systemically studied the influence of boron additive on the high-rate dischargeability of non-stoichiometric La-rich $MmNi_{3.55}Co_{0.75}Mn_{0.4}Al_{0.3}B_x$ ($x = 0$, 0.05, 0.1, 0.2, 0.3; Mm is mischmetal) hydrogen storage alloys [12]. The results show that the addition of boron enhances the activation performance and significantly improves the high-rate capability. Boron-containing double-phase non-stoichiometric hydrogen storage alloys are very promising in some high-power application fields of the Ni/MH battery. However, the pure boron is very expensive and unpractical to be used as additive. B–Ni and B–Fe alloys are cheaper and the transitional metal Fe can substitute for Ni of $LaNi_5$-type hydrogen storage alloy. Besides, B–Ni and B–Fe alloy have much lower melt point than that of pure B and facilitate the homogeneity of alloys.

The objective of this work is to study the phase structure, thermodynamic and electrochemical performances of La-rich $MmNi_{3.55}Co_{0.75}Mn_{0.4}Al_{0.3}B_{0.3}$ hydrogen storage alloys using the cheap B–Ni or B–Fe alloy rather than pure B as additive. At the same time, the influence of different rare

* Corresponding author. Tel.: +86-21-62511070-8805; fax: +86-21-32200534.
E-mail address: yeqhui@mail.sim.ac.cn (H. Ye).

0378-7753/02/$ – see front matter
PII: S0378-7753(01)00869-2

earth composition on these performances of $MmNi_{3.55}Co_{0.75}Mn_{0.4}Al_{0.3}B_{0.3}$ alloys has been studied.

2. Experimental

The $MmNi_{3.55}Co_{0.75}Mn_{0.4}Al_{0.3}B_{0.3}$ hydrogen storage alloys were prepared by a radio frequency levitation melting processing in a copper crucible under an Ar atmosphere. The button ingots were re-melted three times to ensure homogeneity, then the ingots were annealed at 950°C for 6 h under Ar atmosphere. For convenience, B_5, B_6, and B_7 are used as the representation of alloys corresponding to Ce-rich Mm with pure B as additive ($MmNi_{3.55}Co_{0.75}Mn_{0.4}Al_{0.3}B_{0.3}$), La-rich Mm with B–Ni alloy as additive ($MmNi_{3.55}Co_{0.75}Mn_{0.4}Al_{0.3}B_{0.3}$), La-rich Mm with B–Fe alloys as additive ($MmNi_{3.27}Fe_{0.28}Co_{0.75}Mn_{0.4}Al_{0.3}B_{0.3}$) in this paper. For comparison, the performances of B_4 alloy [12], $MmNi_{3.55}Co_{0.75}Mn_{0.4}Al_{0.3}B_{0.3}$ using La-rich Mm and pure B as additive, are also cited in this paper. The La-rich Mm contains 61.7% La, 27.4% Ce, 2.5% Pr, and 8.4% Nd. The Ce-rich Mm contains 31.2% La, 47.4% Ce, 5.0% Pr, and 16.4% Nd. B–Ni alloy contains 18.86% B. B–Fe alloy contains 17.24% B. The B addition amount is calculated based on B content in the B–Ni or B–Fe alloy, accordingly the Ni or Fe will occupy the Ni-site in the $LaNi_5$-type alloys of $MmNi_{3.55}Co_{0.75}Mn_{0.4}Al_{0.3}B_{0.3}$.

The as-prepared alloys were mechanically pulverized into fine powders with an average size of Ø 38–75 μm and less than Ø 38 μm for the electrochemical and X-ray diffraction measurements, respectively.

Crystallographic characterization of the hydrogen storage alloys was carried out by an X-ray diffractometer (Philips X′Pert MPD, Cu Kα). The pressure–composition isotherms were measured with a Sieverts-type apparatus at 333 K by desorption of H_2 gas from the hydride.

The preparation of electrodes and the setup of the tri-electrode cell for electrochemical measurements have been described previously [12]. All electrochemical measurements were carried out at 20°C. The discharge capacity of the electrode was determined by the galvanostatic method. The cutoff potential for discharging was fixed at −0.6 V versus Hg/HgO electrode. To evaluate the rate capability, the discharge capacity of electrode at different discharge current densities was measured. The cutoff potentials for different discharge current densities of 60, 300, 900, 1500 and 3000 mA/g were set to −0.6, −0.6, −0.5, −0.4, and −0.3 V versus Hg/HgO electrode, respectively. The charge transfer resistance of metal hydride electrode was characterized by electrochemical impedance spectra (EIS). EIS was tested in the frequency range of 100 kHz to 1 MHz, with ac amplitude of 5 mV and the electrodes were maintained at the open-circuit state of 50% depth-of-discharge. Potentiostatic discharge technique was used to characterize the hydrogen transfer behavior in the bulk of metal hydride. Rate capability, EIS, and potentiostatic discharge measurements were carried out with Solartron SI1287 Electrochemical Interface connected with a 1255B Frequency Response Analyzer after the investigated electrodes being completely activated (over 40 cycles).

3. Results and discussion

3.1. Structure characteristics

Fig. 1 shows the XRD patterns of $MmNi_{3.55}Co_{0.75}Mn_{0.4}Al_{0.3}B_{0.3}$ hydrogen storage alloys. As seen from Fig. 1, all non-stoichiometric boron-contained alloys (B_4, B_5, B_6 and B_7) show a principal $CaCu_5$-type phase with a small amount of $CeCo_4B$-type phase. Both $CaCu_5$-type phase and $CeCo_4B$-type phase are hexagonal system with *P6/mmm*

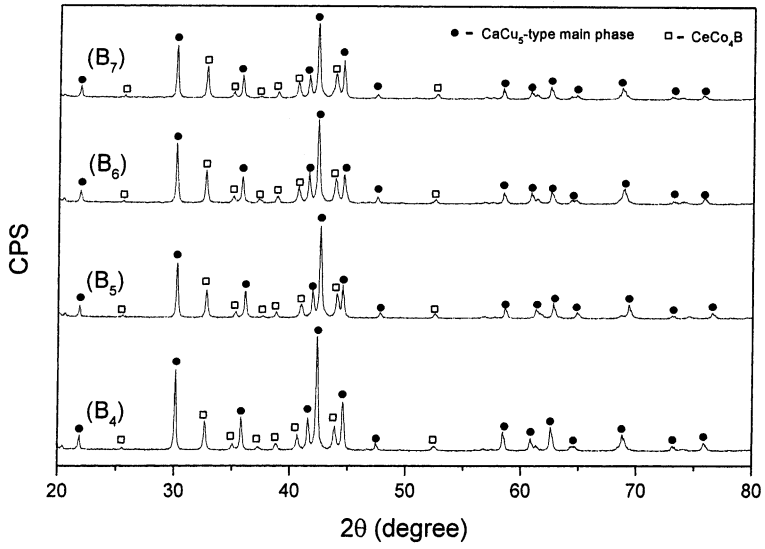

Fig. 1. X-ray powder diffraction patterns of the $MmNi_{3.55}Co_{0.75}Mn_{0.4}Al_{0.3}B_{0.3}$ alloys.

Table 1
Cell parameter and volume of $CaCu_5$-type main phase and $CeCo_4B$-type secondary phase and the abundance of secondary phase in the $MmNi_{3.55}Co_{0.75}Mn_{0.4}Al_{0.3}B_{0.3}$ alloys

Sample	Main phase			Secondary phase			Abundance of secondary phase (%)
	Cell parameter		Cell volume, V (Å^3)	Cell parameter		Cell volume, V (Å^3)	
	a (Å)	c (Å)		a (Å)	c (Å)		
B_4	5.014	4.063	88.45	5.122	6.969	158.32	19.83
B_5	5.069	3.944	87.76	5.323	6.968	170.98	20.38
B_6	5.018	4.067	88.69	5.136	6.970	159.23	22.28
B_7	5.024	4.074	89.05	5.134	6.964	158.96	24.03

space group. Table 1 lists the lattice parameter and the cell volume of main phase and secondary phase of investigated alloys. It is shown that the rare earth composition has a large influence on the cell parameter of main phase and secondary phase. Ce-rich alloy (B_5) shows larger a value and smaller c value of main phase than La-rich alloy (B_4); B_5 also shows larger a value of secondary phase, but it has almost same c value of secondary phase. As a result, compared with La-rich Mm, Ce-rich Mm significantly decreases the cell volume of main phase and increases the cell volume of secondary phase. Whereas, using B–Ni alloy (B_6) or B–Fe alloy (B_7) rather than pure B (B_4) as additive only slightly influence the cell parameter of both phases and somewhat increase the cell volume of them. The cell volume of main phase of B_7 is a little larger than that of B_6 alloy. Since main phase and secondary phase show same space group, it is reasonable to roughly quantify the amount of second phase by using the relative integral intensity of the strongest peak (1 1 1) for $CaCu_5$-type phase and (1 1 2) for $CeCo_4B$-type phase. Here, ratio of integral intensity of (1 1 1) for $CaCu_5$-type phase versus the total integral intensity of both (1 1 1) for $CaCu_5$-type phase and (1 1 2) for $CeCo_4B$-type phase is used as the abundance of secondary phase in the investigated alloys and also listed in the Table 1. As seen from Table 1, the amount of secondary phase of B_6 and B_7 are higher than those of B_4 and B_5. This indicates that using B–Ni or B–Fe alloy, as additive is more favorable for the formation of the secondary phase in the hydrogen storage alloy.

3.2. Thermodynamic characteristics

The pressure–composition isotherms of hydrogen desorption from hydrogenated, pseudo-binary $MmNi_{3.55}Co_{0.75}Mn_{0.4}Al_{0.3}B_{0.3}$ alloys at 333 K are presented in Fig. 2. There is only one plateau for all boron-containing alloys indicating that the secondary phase may not be a hydride-forming phase. From Fig. 2, it is also observed that the dehydrogenation pressure of Ce-rich B_5 is much higher than that of La-rich B_4 alloy. This indicates that the hydride stability of B_5 is lower than that of B_4. The absorption amount of hydrogen for B_5 is also lower than that of B_4 alloy. These may mainly ascribe to the smaller cell volume of $CaCu_5$-type phase in Ce-rich alloy. It is generally accepted that the smaller cell volume of $CaCu_5$-type phase is unfavorable for hydrogen-absorption and also decrease the hydride formation enthalpy. The dehydrogenation pressure of B_6 is very close to that of B_4, which shows that using B–Ni alloy or pure B as additive has less influence on the

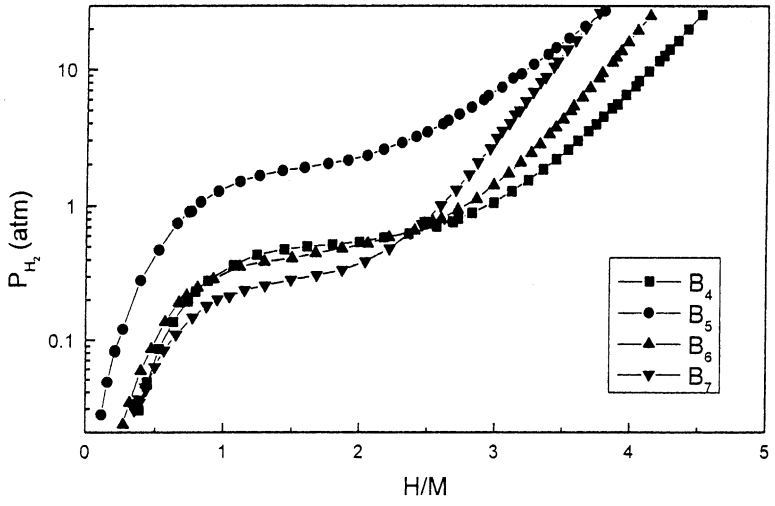

Fig. 2. Pressure–composition isotherms of hydrogen desorption from hydrogenated, pseudo-binary phase of $MmNi_{3.55}Co_{0.75}Mn_{0.40}Al_{0.30}B_{0.3}$ alloys at 333 K.

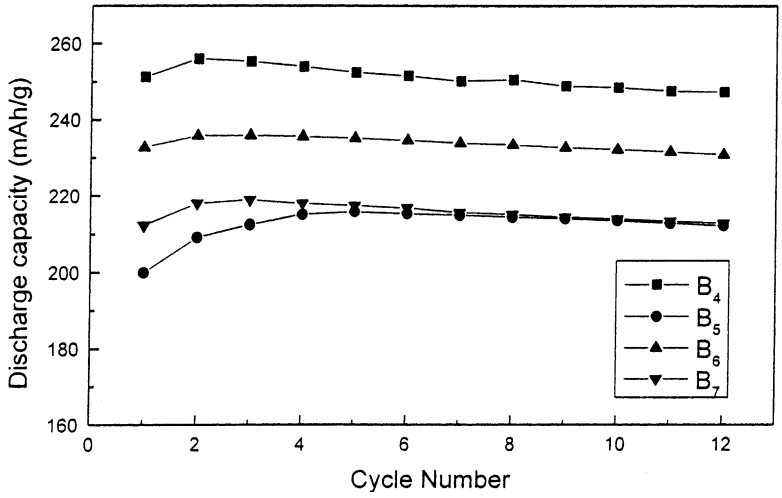

Fig. 3. Activation profiles of $MmNi_{3.55}Co_{0.75}Mn_{0.4}Al_{0.3}B_{0.3}$ metal hydride electrodes.

thermodynamic property of alloys. Whereas, absorption amount of hydrogen for B_6 is less than that of B_4, this can be attribute to the higher amount of secondary phase in the B_6 alloy. Both of hydrogen-absorption amount and dehydrogenation pressure of B_7 are lower than those of B_4 alloy. The former one is ascribe to its having the highest amount of secondary phase of four investigated alloys; the latter one indicates Fe, induced by B–Fe alloy additive, increasing the hydride stability, which is consistent with the increase of cell volume of main phase in B_7 alloy as listed in Table 1.

3.3. Electrochemical characteristics

3.3.1. Activation and maximum capacity

Fig. 3 shows the activation profiles of $MmNi_{3.55}Co_{0.75}Mn_{0.4}Al_{0.3}B_{0.3}$ electrodes. The activation was conducted with charging/discharging cycles under the current density of 60 mA/g. The discharge capacity of all investigated metal hydride electrodes reaches over 90% maximum capacity at first cycle, indicating good catalytic activity. However, the discharge capacities of all $MmNi_{3.55}Co_{0.75}Mn_{0.4}Al_{0.3}B_{0.3}$ electrodes under the current density of 60 mA/g are lower than that of commercial $MmNi_{3.55}Co_{0.75}Mn_{0.4}Al_{0.3}$ hydrogen storage alloy. The maximum discharge capacity of B_4, B_5, B_6, and B_7 is 256, 215.8, 235.9, and 218.9 mAh/g, respectively. The variations of discharge capacity of investigated alloys are consistent with their gaseous hydrogenation/dehydrogenation performances, which are also correlated with the microstructure characteristics of alloys.

3.3.2. High-rate dischargeability

Fig. 4 shows the high-rate dischargeability of the $MmNi_{3.55}Co_{0.75}Mn_{0.4}Al_{0.3}B_{0.3}$ electrodes, where high-rate dischargeability of hydride electrode is expressed with the ratio of the discharge capacity at high current density versus the discharge capacity at 60 mA/g ($C_{y\,mA/g}/C_{60\,mA/g} \times 100\%$, where y is the value of discharge current density).

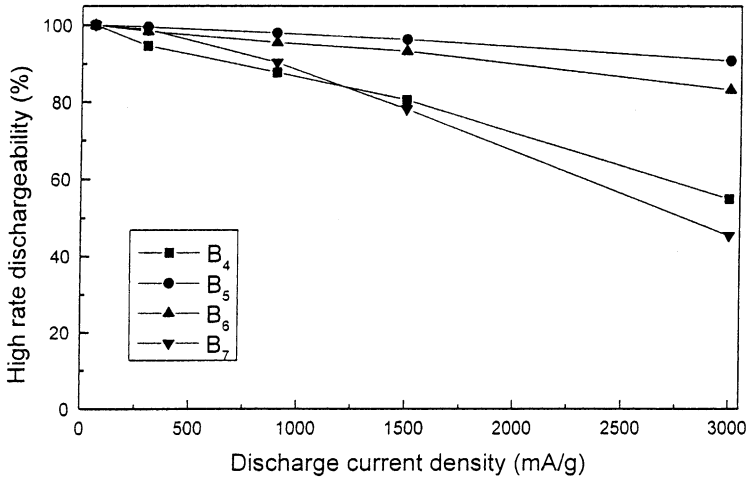

Fig. 4. Relationship between the high-rate dischargeability and the discharge current density of $MmNi_{3.55}Co_{0.75}Mn_{0.4}Al_{0.3}B_{0.3}$ metal hydride electrodes.

As seen from Fig. 4, all investigated metal hydride electrodes show good rate capability. The rate capability of B_7 compound is a little worse than that of B_4 when discharge current density is over 1500 mA/g. Both of B_5 and B_6 show excellent rate capability. For example, the high-rate dischargeabilities of B_5 and B_6 under 3000 mA/g, respectively, reach 90.74 and 83.30%. Both of them can even discharge over 190 mAh/g electrochemical capacity under 3000 mA/g. This displays that both B_5 and B_6 compounds are very suitable for high-power field with a little expense of common-rate capacity.

The electrochemical performances of hydrogen storage alloy are intrinsically determined by its microstructure, thermodynamic and kinetic characteristics under the application environment. The good high-rate dischargeability of investigated $MmNi_{3.55}Co_{0.75}Mn_{0.4}Al_{0.3}B_{0.3}$ compounds can, in microstructure, be ascribed to the formation of secondary phase, which shows very good catalytic activity [11,12]. Comparing B_5 and B_4, we can see that the lower stability of hydride is another large contribution to rate capability. Optimization of Mm-side rare earth composition should further improve the rate capability of AB_5-type hydrogen storage alloy. The good rate capability of B_6 may due to better composition homogeneity than that of B_4; the amount of secondary phase in B_6 is also higher than that of B_4. Though B_7 alloy shows highest amount of secondary phase, but its hydride is more stable than that of B_4. Furthermore, the variation of cell parameter of $CeCoB_4$-type secondary phase may also affect its catalytic activity, which should be studied further. In the electrochemical cell, the rate discharge of metal hydride electrode is mainly determined by the charge transfer process occurring at the metal/electrolyte interface and the hydrogen transfer process in the hydride bulk [13]. Their contribution will be evaluated by electrochemical techniques at follow sections.

3.3.3. Electrochemical impedance spectra

The exchange current density (I_0) of metal hydride electrode reaction used to character the catalytic activity for charge transfer at the metal/electrolyte interface and it can be obtained by the following formula [8]:

$$I_0 = \frac{RT}{FR_d} \quad (1)$$

where R_d, F, R and T are the charge transfer resistance, Faraday constant, gas constant and absolute temperature, respectively. The charge transfer resistance of $MmNi_{3.55}Co_{0.75}Mn_{0.4}Al_{0.3}B_{0.3}$ electrodes was obtained from electrochemical impedance spectra (EIS).

Fig. 5 shows the EIS of $MmNi_{3.55}Co_{0.75}Mn_{0.4}Al_{0.3}B_{0.3}$ electrodes at 50% depth-of-discharge. The electrolyte resistance (R_s), which is mainly determined by the distance between the electrode pellet and the Luggin capillary, was subtracted from EIS in order to get a clear comparison among alloys. It is observed that all EIS consist of two semicircles followed by a straight line at low-frequency. Using

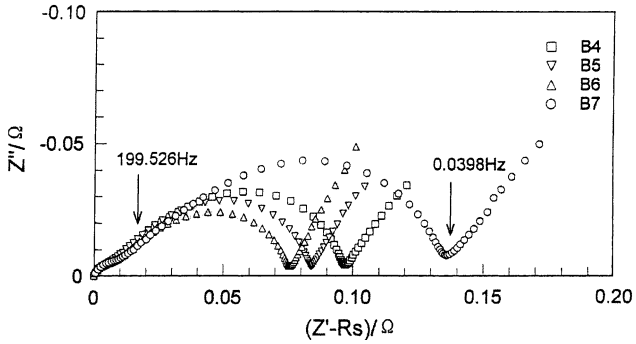

Fig. 5. Electrochemical impedance spectra of the $MmNi_{3.55}Co_{0.75}Mn_{0.4}Al_{0.3}B_{0.3}$ metal hydride electrodes measured at 50% depth of discharge.

the analysis model proposed by Kuriyama et al. [14], the semi-circle in the low-frequency region relates to the charge transfer reaction. The charge transfer resistance of B_4, B_5, B_6, and B_7 through fitting the low-frequency semi-circle of EIS is 0.0754, 0.0665, 0.0575, and 0.1072 Ω, respectively and the I_0 of B_4, B_5, B_6, and B_7 electrode calculated using Eq. (1) is 1116, 1265, 1464, and 785 mA/g, respectively. Compound using B–Ni alloy as additive demonstrates the best catalytic activity of all. The compound with Ce-rich Mm (B_5) also shows better catalytic activity than that of B_4. Though B_7 has more secondary phase, it shows worst catalytic activity. This indicates that the catalytic activity of hydride electrode is not only influenced by the amount of secondary phase. The other reasons such as the characteristics of main phase and the distribution of each phase can also influence this performance.

3.3.4. Potentiostatic discharge

The potentiostatic discharge technique was used to characterize the hydrogen transfer behavior in the $MmNi_{3.55}Co_{0.75}Mn_{0.4}Al_{0.3}B_{0.3}$ electrodes. The investigated electrodes were charged to 120% maximum capacity. After charging and 30 min open-circuit lay-up, the electrode was discharged with +300 mV potential-step. Fig. 6 shows the

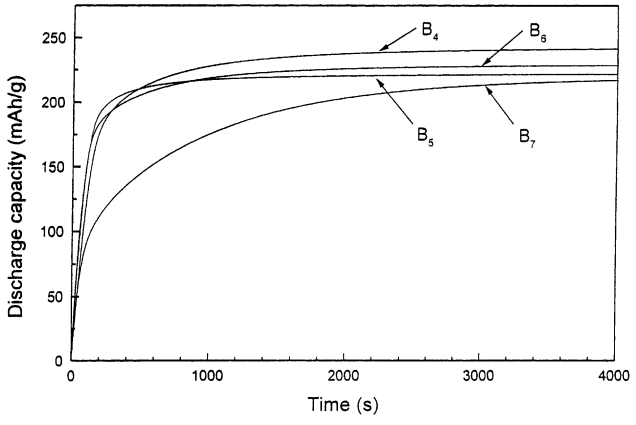

Fig. 6. Relationship between the discharge capacity and the discharge time for $MmNi_{3.55}Co_{0.75}Mn_{0.4}Al_{0.3}B_{0.3}$ electrodes under +300 mV potential-step.

relationship between the discharge capacity and discharge time under potentiostatic condition. It is found that the electrochemical capacities quickly discharge from the electrode at first and then slow down with the time going on. The capacities of electrodes nearly run out after 4000 s discharge. The discharge kinetics of investigated electrodes is clearly exhibited in Fig. 6. For example, the time of discharging 90% capacity of B_4, B_5, B_6, and B_7 electrodes are 626, 269, 498, and 1590 s, respectively. B_5 compound shows the best electrochemical kinetic property.

Zheng et al. [13] reported that metal hydride electrode reaction would be controlled by diffusion-limited mass transfer under a large anodic potential-step. After a long discharge time, the diffusion current will vary with the time according to the Eq. (2):

$$\log i = \log\left(\frac{6FD}{da^2}(C_0 - C_s)\right) - \frac{\pi^2}{2.303}\frac{D}{a^2}t \quad (2)$$

where D is the hydrogen diffusion coefficient (cm^2/s), C_0 the initial hydrogen concentration in the bulk of the compound (mol/cm^3), C_s the hydrogen concentration in the surface of the compound particles (mol/cm^3), a the radius of the spherical particle (cm), d the density of the hydrogen storage alloy (g/cm^3), t the charge or discharge time (s), and i the diffusion current (A/g). From the slope of a plot of $\log i$ versus t, according Eq. (2), D/a^2 may be evaluated, and if the radius of the particle is known, D can be calculated. It should be pointed out that Zheng et al. in Eq. (2) have not considered that the diffusion coefficient generally changes with hydrogen concentration and phase. However, with the assumption that the hydrogen-desorbing system was a homogeneous one, we can get a qualitative comparison of hydrogen diffusion coefficient among different alloys.

Fig. 7 shows the anodic current versus time responses for electrodes after the potential-step with semi-logarithmic plots. It is found that during the period from 94.36 to 98.36% discharge capacity of B_4, B_5, and B_6, the plots show linear segment. As to B_7 the linear segment of plot lasts from 70 to 98.36% discharge capacity. When capacities of the electrodes discharged over 98.36%, the hydrogen retained in the bulk of these compounds is approaching to zero and the side-reaction may lead the relationship between current and time to disobey Eq. (2). From the slope of the linear portion of the corresponding plot in Fig. 7, the ratios of D/a^2 was estimated by using Eq. (2) and listed in Table 2. It is observed that the value of D/a^2 is markedly increased when the alloy adopting Ce-rich Mm. B_6 alloy only has a slightly higher D/a^2 value than that of B_4 and B_7 alloy shows the least value of D/a^2. Assuming all $MmNi_{3.55}Co_{0.75}Mn_{0.4}Al_{0.3}B_{0.3}$ alloy have the similar particle distribution with the average particle radius of 8 μm same to B_4 [12], therefore, the effective diffusion coefficient of hydrogen through $MmNi_{3.55}Co_{0.75}Mn_{0.4}Al_{0.3}B_{0.3}$ electrodes were estimated and also listed in Table 2. The variation of hydrogen diffusion coefficient of compound is well correlated with the hydride stability as discussed in Section 3.2. This result is consistent with the report of Iwakura et al. [15]. The very fast hydrogen transfer in B_5 compound is due to its lowest hydride stability and the existence of secondary phase. The lower hydride stability facilitates the release of bonded hydrogen. The second phase not only improves electrochemical interface reaction, but also provide the fast diffusion path for hydrogen transfer during charge/discharge process. The relatively lower hydrogen diffusion coefficient of B_7 is due to higher stability of its hydride. Using B–Ni alloy rather than pure B as additive only lead to better homogeneity of hydrogen storage alloy, but have little influence on hydride stability, thus, shows less enhance of hydrogen diffusion coefficient.

Table 2
Ratio of D/a^2 and the effective hydrogen diffusion coefficient in the bulk of $MmNi_{3.55}Co_{0.75}Mn_{0.4}Al_{0.3}B_{0.3}$ alloys

Sample	B_4	B_5	B_6	B_7
$D/a^2 \times 10^5$ (s^{-1})	14.93	27.07	16.24	10.59
$D \times 10^{11}$ (cm^2/s)	9.55	17.32	10.39	6.78

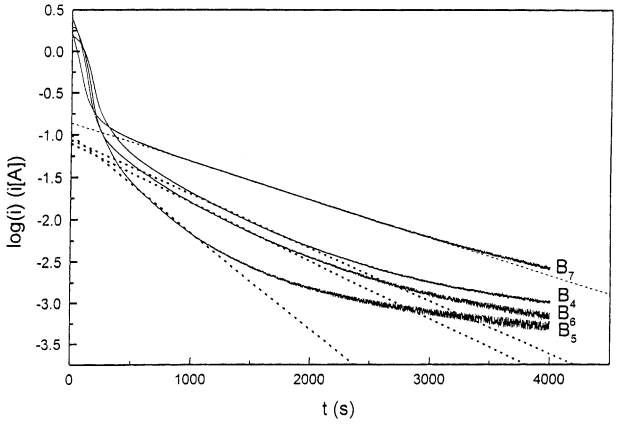

Fig. 7. Anodic current–time responses for $MmNi_{3.55}Co_{0.75}Mn_{0.4}Al_{0.3}B_{0.3}$ metal hydride electrodes after +300 mV potential-step (solid line) and the linear segment of $\log i$ vs. t plot (dashed line).

4. Conclusion

Non-stoichiometric La-rich $MmNi_{3.55}Co_{0.75}Mn_{0.4}Al_{0.3}B_{0.3}$ hydrogen storage alloys using B–Ni or B–Fe alloy as additive and Ce-rich $MmNi_{3.55}Co_{0.75}Mn_{0.4}Al_{0.3}B_{0.3}$ one using pure B as additive have been prepared. The main conclusions are the following: (1) all investigated alloys show $CaCu_5$-type main phase and a small amount of $CeCo_4B$-type phase. Different rare earth (La or Ce)-rich Mm significantly influences the cell parameter of both main phase and secondary phase. Using B–Ni or B–Fe alloy as

additive makes the hydrogen storage alloys more homogenous and more favorable for the formation of secondary phase than pure boron; (2) the hydride stability of Ce-rich alloy is lower than that of La-rich alloys. Using B–Ni alloy rather than pure B as additive shows less influence on the thermodynamic performance. The Fe induced by B–Fe additive increases the hydride stability of prepared alloy; (3) the electrochemical experiments show that all $MmNi_{3.55}Co_{0.75}Mn_{0.4}Al_{0.3}B_{0.3}$ alloys have good activation performance and high-rate dischargeability though the electrochemical capacity is lower than that of commercial $MmNi_{3.55}Co_{0.75}Mn_{0.4}Al_{0.3}$ alloy. The $MmNi_{3.55}Co_{0.75}Mn_{0.4}Al_{0.3}B_{0.3}$ alloy using B–Ni alloy as additive or adopting Ce-rich Mm conduced to excellent rate capability of the hydrogen storage alloys, which can discharge over 190 mAh/g capacity even under the current density of 3000 mA/g, and thus, displays their promising use in the high-power type Ni/MH battery. Electrochemical impedance spectroscopy and potentiostatic discharge measurements indicate that the superior rate capability of alloys is due to high surface electrocatalytic activity and/or fast hydrogen transfer in the bulk of alloys. The electrochemical performances of $MmNi_{3.55}Co_{0.75}Mn_{0.4}Al_{0.3}B_{0.3}$ alloys are well correlated with their microstructure, thermodynamic, and kinetic characteristics.

References

[1] T. Kimura, M. Ikoma, K. Kanamaru, in: Proceedings of the 14th International Electric Vehicle Symposium (EVS-14), Florida, 1997.
[2] P.T. Moseley, J. Power Sources 91 (2000) 1.
[3] P. Gifford, J. Adams, D. Corrigan, S. Venkatesan, J. Power Sources 80 (1999) 157.
[4] K. Wiesener, D. Ohms, G. Benczur-Urmossy, M. Berthold, F. Haschka, J. Power Sources 84 (1999) 248.
[5] J.J.G. Willems, Philips J. Res. 39 (1984) 1.
[6] H. Ogawa, M. Ikoma, H. Kawano, I. Matsumoto, in: T. Keily, B.W. Baxter (Eds.), Proceeding of the 16 International Power Sources Symposium, Vol. 12, Bournmouth, 1989, p. 393.
[7] T. Sakai, H. Yoshinaga, H. Migamura, N. Kuriyama, H. Ishikawa, J. Alloys Comp. 180 (1992) 37.
[8] P.H.L. Notten, P. Hokkeling, J. Electrochem. Soc. 138 (1991) 1877.
[9] Y. Fukumoto, M. Miyamoto, M. Matsuoka, C. Iwakura, Electrochim. Acta 40 (1996) 845.
[10] H. Ye, H. Zhang, J.X. Chen, T.S. Huang, J. Alloys Comp. 308 (2000) 163.
[11] M. Tadokoro, M. Nogami, Y. Chikano, M. Kimoto, T. Ise, K. Nishio, N. Fukukawa, J. Alloys Comp. 192 (1993) 179.
[12] H. Ye, H. Zhang, W.Q. Wu, T.S. Huang, J. Alloys Comp. 312 (2000) 68.
[13] G. Zheng, B.N. Popov, R.E. White, J. Electrochem. Soc. 142 (1995) 2695.
[14] N. Kuriyama, T. Sakai, H. Miyamura, I. Uehara, H. Ishikawa, J. Alloys Comp. 202 (1993) 183.
[15] C. Iwakura, T. Oura, H. Inoue, M. Matsuoka, Y. Yamamoto, J. Electroanal. Chem. 398 (1995) 37.